Investigation of mechanical energy harvesting cycles using ferroelectric/ferroelastic switching

Wenbin Kang[1], Lulu Chang[2] and John Huber[1*]

1. Department of Engineering Science, University of Oxford, Parks Rd, OX1 3PJ, United Kingdom
2. College of Aerospace Engineering, State Key Laboratory of Mechanics and Control of Mechanical Structures, Nanjing University of Aeronautics and Astronautics, Nanjing, Jiangsu, China

*Email: john.huber@eng.ox.ac.uk

Abstract

Piezoelectric energy harvesters have been widely developed in last decade due to their simplicity and practicality, but they suffer from low energy density. To increase the energy density, ferroelectric/ferroelastic switching could be an effective alternative energy harvesting approach. However, the nonlinearity and irreversibility of ferroelectric switching produces difficulty in establishing a stable working cycle. In this work, novel, practical and stable energy harvesting cycles using ferroelectric/ferroelastic switching are established and explored under quasi-static experimental conditions. A prototype device with a simple 'sandwich' configuration is tested. The results show that the cycle energy density can reach 11 mJ/cm^3 under tensile loading and 3.2 mJ/cm^3 under compression, demonstrating great potential for practical applications.

Key words: Energy harvesting, Mechanical design, Ferroelectric/ferroelastic switching, Optimization

1. Introduction

The increasing energy demands of mobile electronics, wearable devices, biomedical implants and wireless sensing are challenging the capabilities of battery technology. The limited size, lifespan and inflexibility of batteries cannot satisfy all the requirements of these always-on electronics. Some new technologies, such as the fifth generation of wireless communications technologies (5G) and Internet of things [1], also need efficient energy use for data transmission and actuation. Thus it becomes attractive and promising to convert various ambient energy sources, such as solar, thermal, and vibrational or kinetic energy, into electricity [2-6], with the advantages of generating renewable and sustainable energy and reducing the costs of battery replacement or wired systems. Vibration energy is relatively common in the built environment because it is a natural consequence of human motion, and environmental fluid flows of water or air. There are three widely used conversion mechanisms already found in service: piezoelectric, electromagnetic and electrostatic[7-9]. Among these, the piezoelectric energy harvester (PEH) has the advantages of high output and simplicity. Thus there has been great interest in improving the performance of PEHs [3, 9, 10]. A comprehensive review of piezoelectric and ferroelectric materials, advanced improvements of piezoelectric ceramics and composites and the optimization approaches for complex piezoelectric energy harvesting systems have been presented in previous work [11].

PEHs usually take the form of bimorph or unimorph cantilevers, with top and bottom electrodes in d_{31} mode, or interdigitated electrodes (IDEs) in d_{33} mode [12-16]. Challenges include controlling the resonant frequencies, and improving the output power density. Research on resonance has focused on structural modifications such as the use of circular diaphragms or zigzag beams, and thereby improving the energy output [17-19]. Other researchers have worked on improved power density through material choice, using two-dimensional materials and biomaterials [20-25]. Additionally, multi-degree-of-freedom PEHs [26-28] and two- or three-dimensional energy harvesters [29-31] have been investigated in order to broaden the bandwidth and energy output. Magnetically assisted mono-stable nonlinear [32-34] and bi-stable nonlinear mechanisms [35, 36] have also been introduced into PEH technology to adapt to low frequency ambient vibrations. Similar capabilities were achieved using frequency up-

conversion mechanisms [37-40], or combined piezoelectric and electromagnetic energy harvesters[41, 42].

Ferroelectric materials, which include many of the common piezoelectrics, have strong and reversible permanent dipole moments and can be applied advantageously to energy harvesting [4, 6]. Ferroelectrics have been used to improve the output power in PEHs [12, 43-46], as well as pyroelectric energy harvesters and even photovoltaics [47-51]. With the advance of nano-technology, ferroelectrics are also used in emerging energy harvesting mechanisms employing triboelectricity. Wang et al. [52] developed triboelectric nanogenerators based on the coupling of triboelectrification and electrostatic effects. Ferroelectric layers are included to improve device stability [53].

Nonlinear ferroelectric/ferroelastic switching induced by electric field and stress offers the potential for high power density in energy harvesting [54-58]. Several theoretical high-performance ferroelectric energy harvesters have been developed in recent years including a working cycle [59] in which a polycrystalline ferroelectric material is partially depolarized with stress, and then repolarized with combined electromechanical loading and an external bias field. This energy harvesting system has the advantage that it employs standard bulk ferroelectrics and has the potential to be realized in various kinds of structural forms, though there is complexity in controlling the external bias voltage. Warkentin et al. [54] further analysed and optimised this working cycle using a ferroelectric switching model.

The present work focuses on establishing and optimising a quasi-static ferroelectric/ferroelastic cycle that converts mechanical to electrical energy. Novel and practical energy harvesting cycles are explored in which the state of the ferroelectric is prepared by an initial step of partial poling to produce a pre-poled condition. States with 30% - 100% of the full remanent polarization are produced in a soft, lanthanum doped lead zirconate titanate (PLZT) wafer. The pre-poled wafer is then adhered to a substrate before completing the poling process; this produces a state of residual stress that enhances ferroelastic switching at low levels of externally applied stress. Electromechanical energy harvesting cycles driven by stress are then presented. Two distinct kinds of energy harvesting cycles are identified. In the first, bending of the substrate is used to induce tension in the ferroelectric wafer, causing partial depolarization; relaxation of the mechanical load enables switching back to a near fully polarized state. In the second type of cycle, bending loads are used to produce compression in the wafer, increasing the polarization from a partially polarized starting state. Then, upon relaxing the mechanical loads, the wafer returns to the partially polarized state. An opposing electric field is used during energy harvesting to simulate an electrical load, and the effect of this on device performance is explored. The quasi-static tests reveal a functioning energy harvesting cycle with great potential for the development of high energy density devices.

2. Concept and design

Ferroelectric/ferroelastic switching can induce changes of electric displacement of the order of 0.1 C/m^2, while the piezoelectric effect typically accounts for changes only of order 10^{-3} C/m^2. Therefore, ferroelectric switching could generate greater charge and energy flows, at the cost of non-linearity, and with the challenge of creating a stable, stress driven, energy harvesting cycle. Specifically, a depolarized ferroelectric cannot normally be repolarized with stress alone; electric field is required for the poling process. Thus, a combination of stress and electric field is normally needed to achieve stable cycles.

Some theoretical designs of ferroelectric energy harvesters [54, 55] solved the problem of cycle stability by using a bias electrical field, which breaks the symmetry of the unpoled state, and allows the action of stresses to drive a repolarization process that is effectively “directed” by the bias field. However, the use of a bias field is a design complication which may be disadvantageous in some contexts, because it requires additional electronic components to apply and control the bias field at the appropriate time in the stress cycle. Instead, making use of the interactions of grains in polycrystalline ferroelectrics, internal bias fields can direct the repolarization process. One approach is to partially depolarize the ferroelectric element while applying mechanical constraint, leaving residual stress and internal electric fields that can assist repolarization. In this case, a ferroelectric/ferroelastic switching

cycle can be produced using a mechanical load cycle without the need for an externally applied bias field during repolarization.

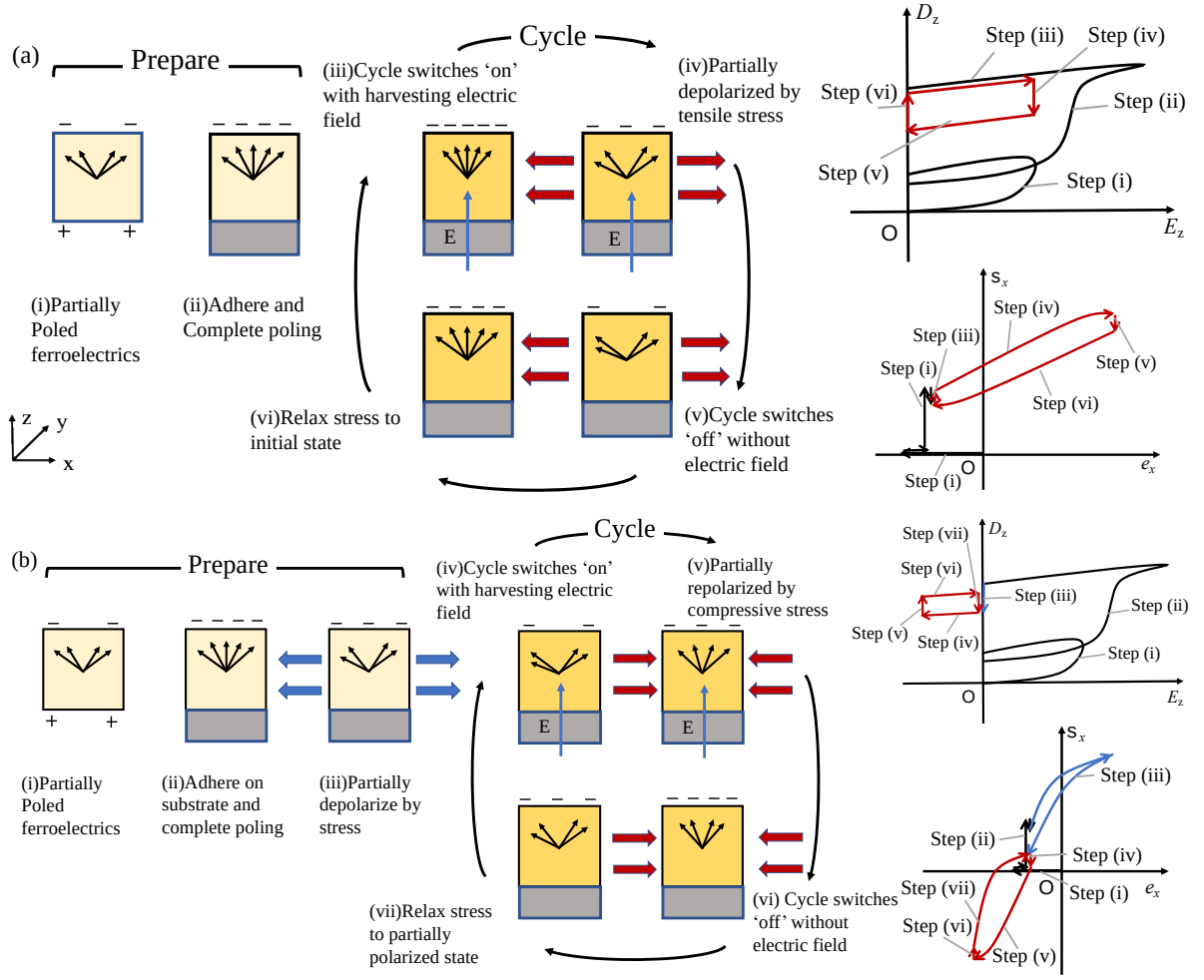

Figure 1. Preparation and ferroelectric energy harvesting cycles (a) Using cyclic tensile loading with a substrate (b) Using cyclic compressive loading with a substrate. Black arrows indicate the polarization distribution. Red arrows indicate mechanical loading.

Two kinds of ferroelectric energy harvesting cycles based on the concept of internal bias fields are presented in fig.1. These use cyclic uniform tensile or compressive loads applied along the *x*-axis to control the *z*-axis polarization. The cycle shown in fig. 1(a) uses tensile stress. The ferroelectric element is first partially poled along *z*-axis, then adhered to a stiff substrate before the poling is completed. When a cyclic tensile load is applied along the *x*-axis, there is a resulting cyclic polarization change along the *z*-axis. Since the ferroelectric element is mechanically coupled to the substrate, strain along the *x*-axis induced by increasing polarization is resisted by the substrate, resulting in tensile residual stress in the ferroelectric. Cracking of the ferroelectric element can be avoided by controlling the degree of partial poling at step (i). An alternative way to exploit internal fields can be seen in fig. 1(b), which uses a compressive load cycle. In the preparation stage, the ferroelectric ceramic is first partially poled before it is bonded on the substrate, it is then fully polarized, which produces a state of tensile residual stress along the *x*-axis. In a final preparation step, a single tensile loading cycle is used to partially depolarize the ceramic. This depolarization reduces the residual tensile stress. Afterwards, a compressive cyclic load can be applied to the ferroelectric ceramic layer to drive the cyclic change in polarization. The compressive external load has the effect of reducing the residual tensile stress in the ferroelectric element and putting the material into compression along the *x*-axis, which will result in an increase in polarization. Relaxing the compressive stress in the ferroelectric element restores the partially depolarized state. Displacement of charge is associated with the change in polarization, providing the ability to do work against an electrical load (e.g. providing power to a load, such as charging a battery). The corresponding change of electric displacement versus electric field, and stress

versus strain are sketched in fig. 1, where red arrows indicate the cyclic hysteresis loop with positive mechanical work input and electrical work output. The method of fig. 1(b), using compressive stress, may be preferable in reducing fatigue damage to the ferroelectric element.

For practical applications, bending loads applied to the substrate can be used to produce the cyclic mechanical loading of the ferroelectric element. It is then desirable to generate as uniform a stress on the ferroelectric material and as great a charge displacement as possible. This leads to the choice of a low thickness ferroelectric wafer with large electrode area. A further practical advantage of the low-thickness layer is that this limits the applied and generated voltages. In general, the energy generated per cycle is proportional to the volume of the ferroelectric element. Thus it is not necessarily advantageous to use thin films as this would constrain the energy produced per unit area of the device. In this work, a wafer (~ 300μm thick) of bulk ferroelectric ceramic is used, with a 1mm thick substrate. Uniformity of the load conditions along the *x*-axis is achieved by applying four-point bending on the substrate, producing uniform bending moment.

3. Fabrication and test arrangements

The ferroelectric 8/65/35 PLZT was chosen as the active layer for energy harvesting due to its low coercive field and stress. The material has a 110°C Curie temperature, 68 GPa Young's modulus, and coercive field of 0.36 MV/m, with 0.25C/m^2 remanent polarization at room temperature and typical grain size of about 1μm [60]. The fine grain size contributes to increased fracture toughness, which is expected to be advantageous when tensile loads are used. 8/65/35 PLZT is a relaxor ferroelectric that, in the unpoled state, displays nano-polar regions. During poling, these regions grow to form domains and the poled or partially poled material exhibits ferroelectric behaviour, similar to a rhombohedral ferroelectric. The material response to stress displays ferroelastic switching due to reorientation of domains[60]. In the present work, the energy harvesting device exploits both ferroelastic and ferroelectric switching. The layered structure of the energy harvester is shown in fig. 2(a,b), where the active ferroelectric layer is adhered to a 1mm thick tool-steel beam using conductive adhesive. Initially, PLZT wafers were cut from the bulk ceramic to dimensions of 38 x 4 x 0.33mm. The wafers were electroded and partially poled, off the substrate, to 30%, 50%, 75% and 100% of the full remanent polarization of PLZT. Electrodes were removed, and the wafers were bonded to a 68 x 4 x 1mm substrate, after which an upper electrode was reinstated on the free surface of the wafer. A ground voltage wire was connected to the conductive substrate. The upper electrode was wired to the external circuit.

The four-point bending was applied using a Deben microtester, with the arrangements shown in fig. 2(c), and a 5mm spacing between each pair of ceramic loading pins. Mechanical loading $F/2$ is applied by each pin to the substrate. We use the convention that $F > 0$ results in tensile loading of the PLZT layer, while $F < 0$ results in compression. Variation of the total force amplitude, F, was explored during testing as this could change the energy harvesting performance. To test various force amplitudes, a triangular waveform of mechanical loading was applied as shown in fig. 2(d). Charge measurements were implemented using a high capacitance electrometer inserted in the ground side of the circuit, while voltages on the upper electrode of the ferroelectric were computer controlled through a high voltage amplifier, see fig 2(e,f). The applied electric field can be written as λE_0, where E_0 is the coercive field and λ is a factor to represent various electrical loads. For both energy harvesting methods, the energy harvesting cycle was tested by applying the following pattern of loading: i) Apply voltage to the upper electrode with the lower electrode grounded to produce electric field λE_0, switching the cycle 'on'. This electric field provides the load against which the energy harvester works, referred to here as the "harvesting electric field". ii) With the harvesting electric field held constant, apply a mechanical loading force increasing to $F/2$ at each pin. This force drives in-plane tension or compression of the ferroelectric wafer. iii) With the loading pins held fixed (i.e. at approximately constant loading), reduce the applied electric field to zero. This switches the energy harvesting part of the cycle 'off'. iv) Reduce the mechanical load to zero. Leakage current tests were carried out to check for leakage across the ferroelectric element. Leakage was found to increase with the electric field, and was dependent on the

quality of the applied electrodes; the leakage values were small enough to have negligible effect on the measurement of electric displacement changes.

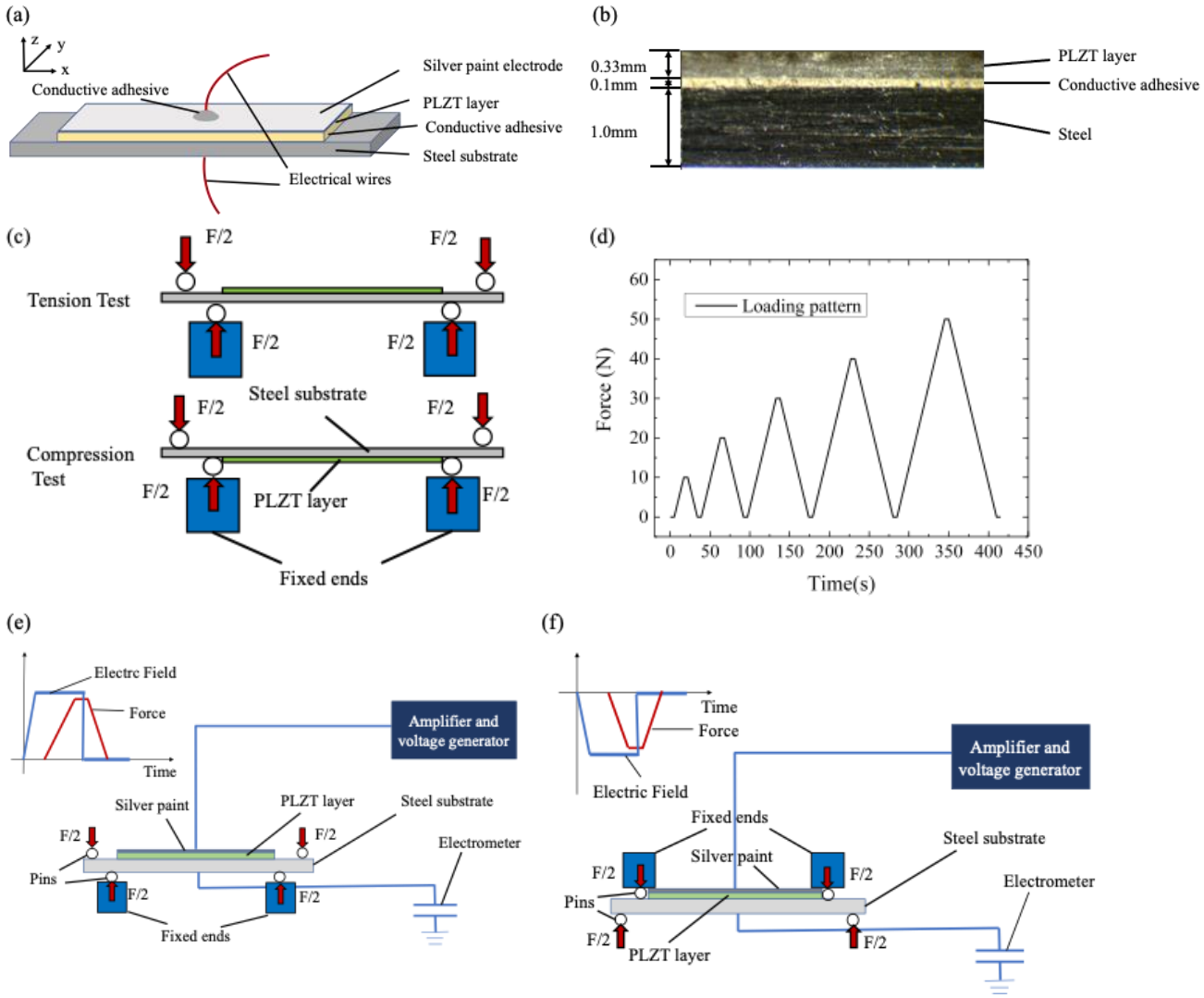

Figure 2. (a) Arrangement of the energy harvester. (b) Optical micrograph of the layered structure. (c) The four-point bending tests using compressive load stress and tensile loading. (d) The loading path for tension and compression tests. (e) Arrangement of energy harvesting using cyclic tensile loading. (f) Arrangement of energy harvesting using cyclic compressive loading.

4. Results and discussion

4.1 Preliminary tests at zero electrical load

Initial tests were conducted without electrical load ($\lambda = 0$) to investigate the behavior of fully or partially pre-poled specimens under quasi-static mechanical loading. The electric displacement versus mechanical load curves are shown in fig. 3 (tension) and fig. 4 (compression). The corresponding mechanical force versus loading pin displacement is also presented. Note that the 100% pre-poled specimens do not have residual tensile stress, having been fully poled off the substrate, while the 75%, 50% and 30% pre-poled specimens are expected to have increasing values of residual tensile stress, as poling was completed on the substrate in these cases. The peak absolute value *F* was varied in the range from 10N to 50N. From fig. 3 and fig. 4, it can be seen that greater electric displacement changes occur in the samples with less pre-poling.

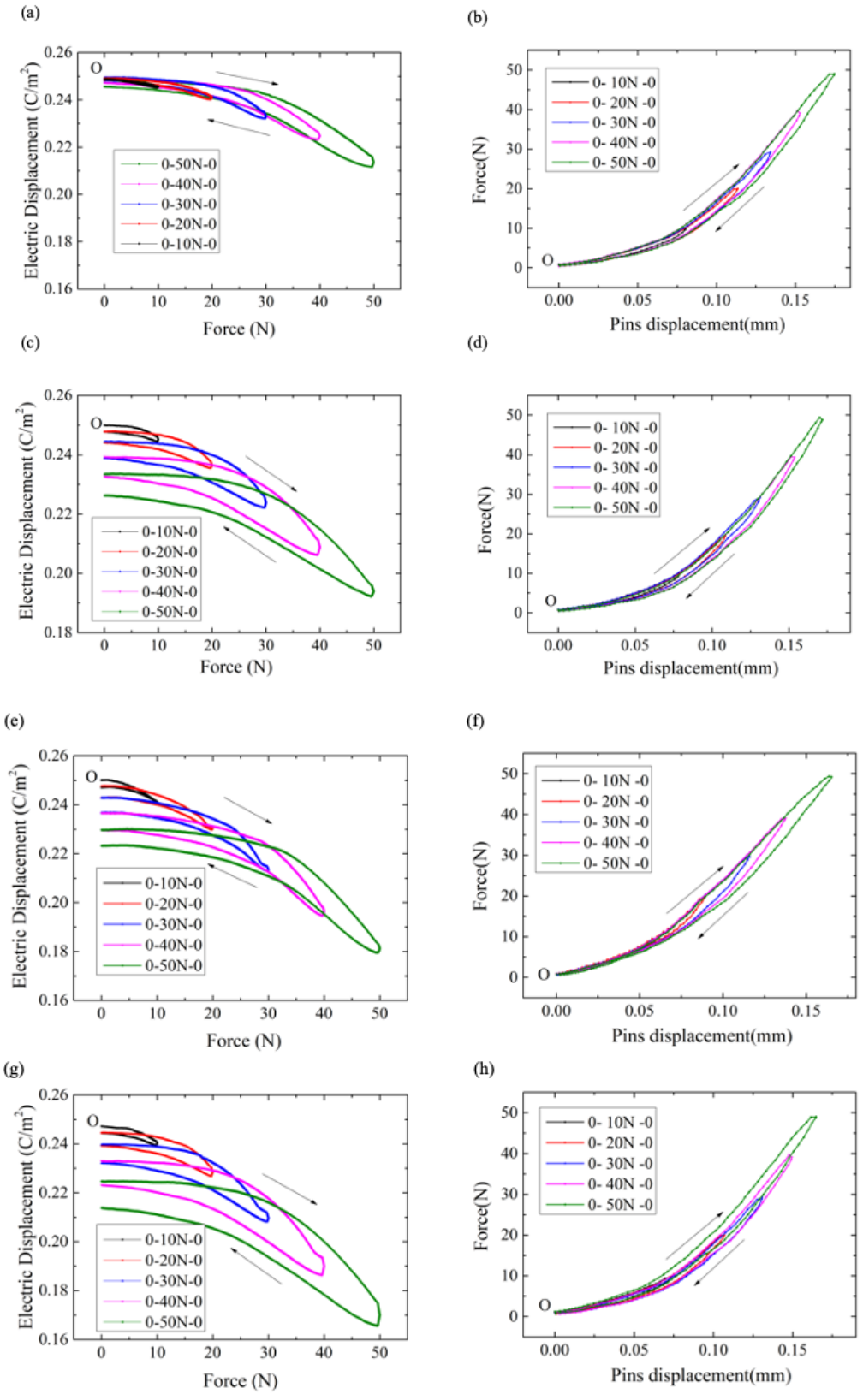

Figure 3. The behavior of specimens under tensile stress. (a,c,e,g) Electric displacement versus force on pins; (b,d,f,h) Force versus pin displacement. Pre-poling states as follows: (a,b) 100%, (c,d) 75% (e,f) 50% (g,h) 30%.

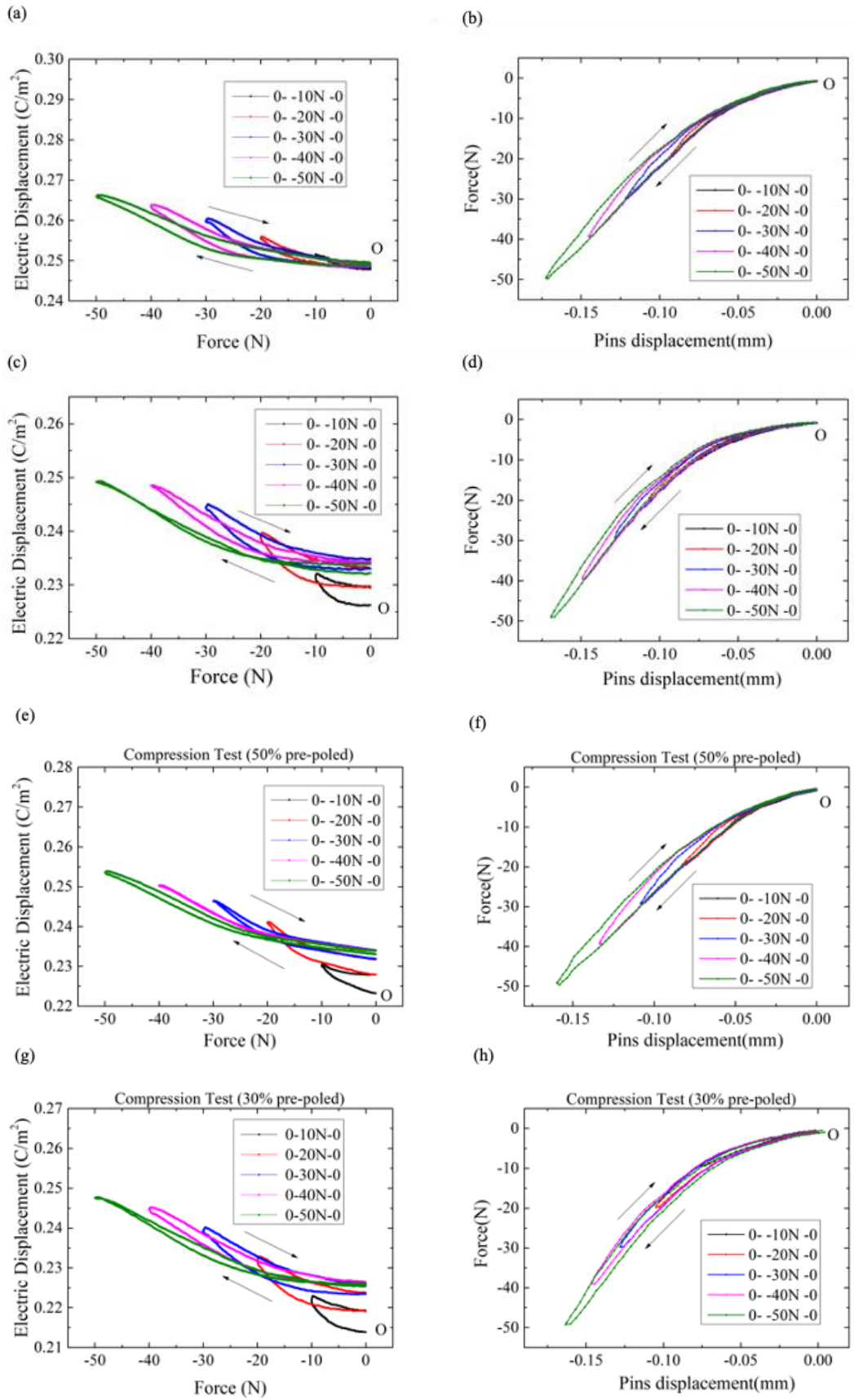

Figure 4. The behavior of specimens under compressive stress. (a,c,e,g) Electric displacement versus force on pins; (b,d,f,h) Force versus pin displacement. Pre-poling states as follows: (a,b) 100%, (c,d) 75% (e,f) 50% (g,h) 30%.

Figs. 3(a,b) show the behavior of 100% pre-poled specimens under tensile stress at zero electrical load. Mechanical loading partially depolarizes the PLZT layer while unloading allows the polarization to switch back, as seen in fig. 3(a). Non-linearity of the response becomes pronounced once the force magnitude reaches 30N, suggesting the stretching of PLZT layer triggers ferroelastic switching. Upon unloading, the partially depolarized wafer is compressed by interaction with the substrate causing the polarization to switch back towards the initial state. Some electric displacement change due to the piezoelectric effect is also observed but there is additional ferroelastic/ferreoelctric switching due to the applied stress.

In the 30%-75% partially pre-poled specimens, residual tensile stress can assist switching and hence enhance polarization changes in the PLZT wafer. When the 75% pre-poled samples were tested in tension, this resulted in increased changes in electric displacement, see fig. 3(c). However, upon unloading the force, the fully polarized material state is not restored: some of the material has not switched back. A bias electric field would be needed to restore the initial polarization value. In fig. 3(c), pin loads as low as 10N induce non-linearity and switching, due to the assistance of residual tensile stress. The results for 50% pre-poled and 30% pre-poled wafers are given in fig. 3 (e-h). These show similar features to the results for the 75% pre-poled sample, with the residual tensile stress assisting depolarization. There are visible jumps in displacement and electric displacement at peak force in fig. 3, especially at high load amplitudes; this can be attributed to the effect of friction between the ceramic loading pins and the steel substrate causing hysteresis where the direction of motion reverses. From all the results in fig. 3 it is evident that working cycles with cyclic mechanical load producing non-linear changes in electric displacement can be achieved using tensile stress.

Next, compare the results of fig. 3 with similar tests in which the loading of the PLZT is compressive, presented in fig. 4. By contrast with the tensile loading results, the compression tests of fig. 4(a) have relatively small polarization changes; this may be expected because the material is already in a near saturated state of polarization and transverse compression cannot drive the polarization much further. However, in the 75%-30% pre-poled states, fig. 4(c-h), significant polarization changes are seen, and closed cycles of force versus electric displacement can be achieved in some cases. Initial loading at small amplitudes (10-20N) ratchets up the electric displacement a little, but subsequent loading to 30-50N produces closed cycles. The results assist the selection of a working cycle to optimize the closed-circuit electric displacement change, enabling a compromise to be struck between stability or closure of the cycle and the magnitude of the polarization change achieved in each cycle. Good cycle stability with significant polarization switching can be achieved in the case of 30% pre-poling with 50N cyclic load.

4.2 Energy harvesting using tensile stress

We now consider cyclic tensile loading of the energy harvester, while imposing an electric field that simulates an external electrical load. For brevity, results for a 30% pre-poled sample are shown. The electrical load is switched ‘on’ during the energy harvesting part of the cycle and then switched ‘off’ while the mechanical load is relaxed to restore the initial state. Measurement of the working cycles was carried out for tensile loading cases with a harvesting electric field λE_0, where E_0 is the coercive field of PLZT. An example of an energy harvesting cycle is shown in fig. 5, in which the electrical loading was set to $\lambda = 1.0$ and the amplitude of the applied force was varied in the range 10N to 50N.

Each cycle starts at the point marked ‘O’. The relationship between electric displacement and the force applied on pins is shown for the tensile loading case in fig. 5(a). The cycle proceeds clockwise from point ‘O’; vertical segments of the force-electric displacement response indicate rapid changes of electric displacement due to switching the electric field ‘on’ or ‘off’. The curved segments correspond to the application or removal of the mechanical loading. The same cycles are plotted as voltage versus charge on the electrode in fig. 5(b); here straight horizontal segments indicate mechanical loading or unloading at constant voltage, while the curved portions of the cycle show change in electric displacement induced by switching the electric field ‘on’ or ‘off’.

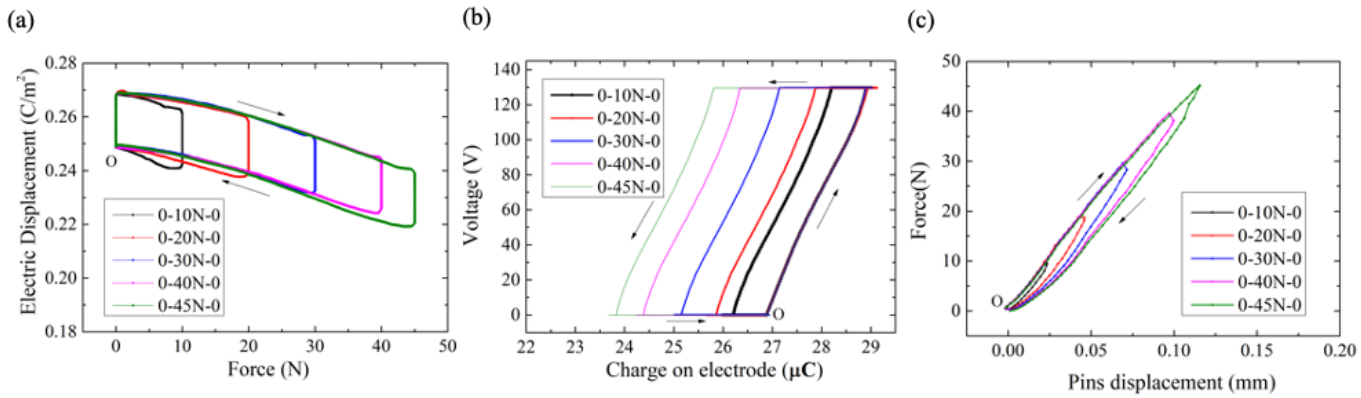

Figure 5. An example of energy harvesting cycle using tensile stress harvesting electric field of magnitude $1.0E_0$ for 30% pre-poled material. (a) Electric displacement versus force. (b) Voltage versus charge on electrode. (c) Force versus pins displacement.

In fig. 5(a), the magnitude of the electric displacement change is greater than 0.03C/m^2. This magnitude is significantly less than that in the closed-circuit case at zero electrical load of fig. 3: the electrical load resists ferroelectric/ferroelastic switching somewhat. However, the electric displacement changes are still much greater than those typically achieved in PEHs. The enclosed area in each loop of fig. 5(b) represents the electrical energy output per cycle. The corresponding mechanical energy input can be estimated using the enclosed area of the force versus displacement curves in fig. 5(c).

The key parameters controlling the energy output of the cycle are the force amplitude and the electrical load. Several factors affect the choice of these parameters. Increasing the force amplitude drives increased switching to produce more energy output. However, high force may damage the ferroelectric wafer, especially in the tensile mode of operation. During operation, cracks were observed to form in the ferroelectric wafer in the 30% and 50% pre-poled specimens when $F > 40$N and $\lambda > 0.8$ in some cases. Lines of dark contrast were seen through the back-lit translucent material when cracks formed. Furthermore, setting the force amplitude too high can result in an unstable cycle that rapidly degrades, reducing the energy output. Another key parameter is the harvesting electric field, simulating an electrical load. In practical applications the field amplitude will be determined by the nature of the external circuit; this can be controlled to a degree by choosing the load components that condition the electrical output of the harvester for downstream use. Increasing λ can result in increased electric work, but can also reduce the extent of mechanically induced switching: an optimum should be found if work output is to be maximized. Additionally, when λ exceeds unity, the field strength becomes great enough to cause extensive ferroelectric switching that can overwrite the engineered material state of the energy harvester.

To investigate further, the energy output per cycle, and electric displacement change under tensile stress, are shown versus the mechanical loading F and electrical load factor λ in fig. 6. These results are for 30%-100% pre-poled specimens and summarize a series of tests in which λ and F were varied in the ranges $0.2 \leq \lambda \leq 1$ and $10 \leq F \leq 50$N. The energy output typically increases with force amplitude and the applied field strength, as may be expected, but there are some exceptions where increasing the field strength too far blocks switching and results in reduced energy output. The energy output per cycle reaches a maximum of 295 μJ for the 100% pre-poled specimen with $\lambda = 1.0$ and $F = 50$N. Comparing this with the 30% pre-poled specimen in fig. 6(g) indicates that the energy output can increase to over 405μJ by exploiting the partially poled state. Although increasing the harvesting electric field generally increases energy output, fig. 6(b) shows that it can reduce the electric displacement change.

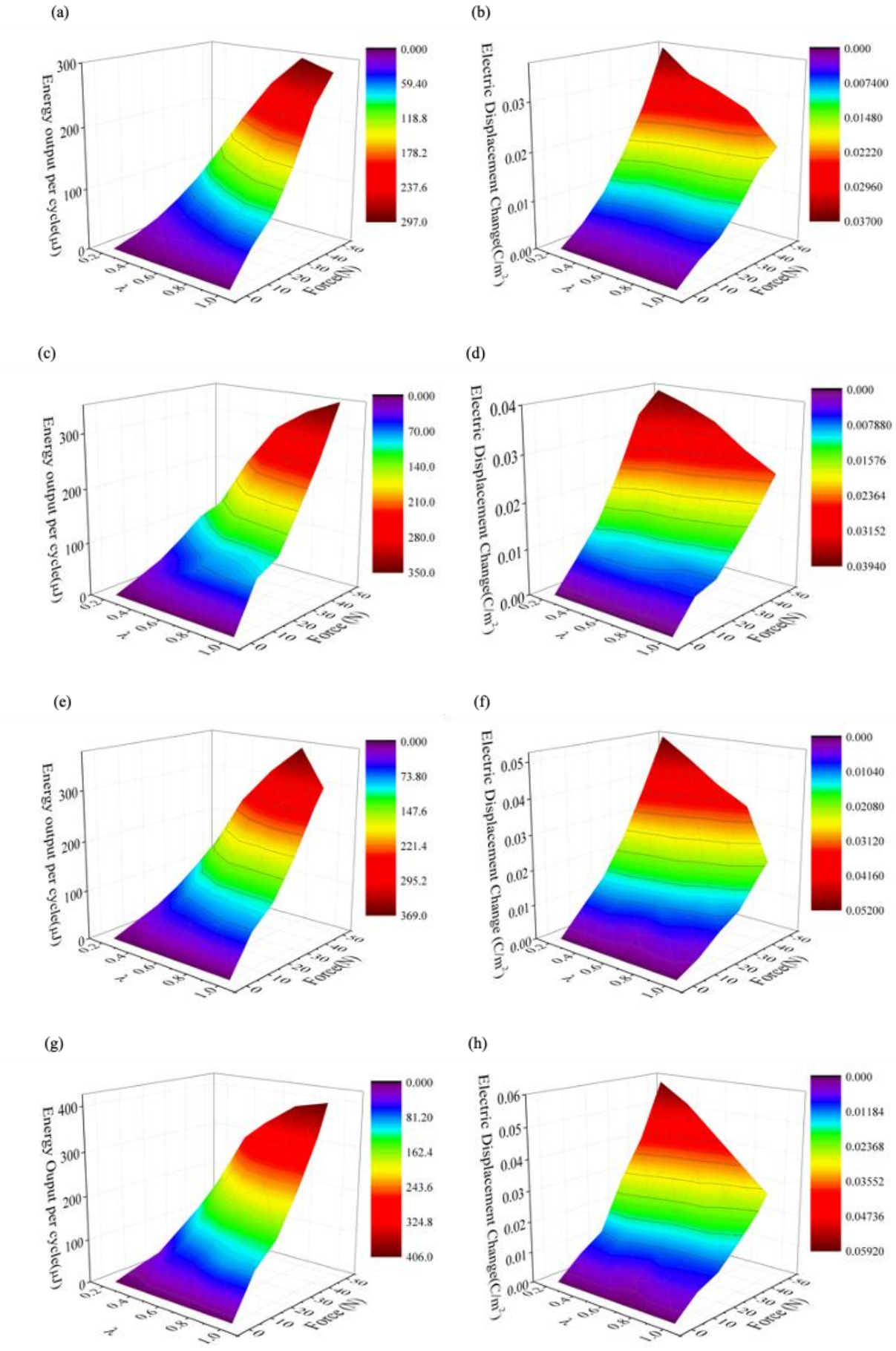
(a)
Energy output per cycle(μJ)
300
200
100
0
0.2
0.4
0.6
0.8
1.0
λ
0
10
20
30
40
50
Force(N)
0.000
59.40
118.8
178.2
237.6
297.0
(b)
Electric Displacement Change(C/m²)
0.03
0.02
0.01
0.00
0.000
0.007400
0.01480
0.02220
0.02960
0.03700
(c)
Energy output per cycle(μJ)
0.000
70.00
140.0
210.0
280.0
350.0
(d)
Electric Displacement Change(C/m²)
0.04
0.03
0.02
0.01
0.00
0.000
0.007880
0.01576
0.02364
0.03152
0.03940
(e)
Energy output per cycle(μJ)
0.000
73.80
147.6
221.4
295.2
369.0
(f)
Electric Displacement Change (C/m²)
0.05
0.04
0.03
0.02
0.01
0.00
0.000
0.01040
0.02080
0.03120
0.04160
0.05200
(g)
Energy Ouput per cycle(μJ)
400
300
200
100
0
0.000
81.20
162.4
243.6
324.8
406.0
(h)
Electric Displacement Change(C/m²)
0.06
0.05
0.04
0.03
0.02
0.01
0.00
0.000
0.01184
0.02368
0.03552
0.04736
0.05920

Figure 6. Energy output and electric displacement performance of the energy harvesters in tensile loading with various operating conditions: (a,c,e,g) Energy output per cycle versus peak force and harvesting electric field magnitude, (b,d,f,h) Corresponding magnitude of electric displacement change in each cycle. Pre-poling states as follows: (a,b) 100%, (c,d) 75% (e,f) 50% (g,h) 30%.

The peak electric displacement change reduces from 0.037C/m^2 with $\lambda = 0.2$ to 0.019 C/m^2 when $\lambda = 1.0$ for 100% pre-poled specimen. Steady increases in the maximum energy output per cycle and electric displacement change at the peak mechanical force are seen as the degree of pre-poling is reduced. However, to avoid cracking, the peak mechanical load was reduced to 45N when $\lambda > 0.6$ for 50% pre-poled specimen and when $\lambda > 0.4$ for 30% pre-poled specimen. Based on this investigation the 30% pre-poled samples gave the greatest energy output per cycle, at 410 μJ and avoided cracking of the ferroelectric element during the final poling process. Samples pre-poled by less than 30% of the full remanent polarization typically cracked when fully poled on the substrate, indicating that in these cases the residual stresses developed in the final poling process could exceed the tensile strength of the ceramic.

4.3 Energy harvesting using compressive stress

The energy harvesting performance under cyclic mechanical compressive loading, with the applied electric field reversed ($\lambda < 0$), is studied in this section. The working cycle is similar to the cycles under tensile stress: the electric field is switched 'on' during the energy harvesting part and switched 'off' when the force is relaxed to restore the initial material state. The peak applied force was varied in the range -10N to -50N.

Fig. 7(a-c) shows typical working cycles, these being obtained using compressive loading with λ = -0.3 for the 30% pre-poled specimen. Starting at the point marked 'O' the cycle proceeds clockwise in fig 7(a). The magnitude of the electric displacement change in this working mode with a peak force of -50N is about 0.025 C/m^2. This is less than that of the tensile cycle, but still a significant improvement relative to typical PEHs. Comparing with the cases at zero electric load in fig. 4, the resistance to switching caused by the electrical load is evident. An open shape of hysteresis curve in fig. 7(c) indicates a greater mechanical energy input in this case, and the enclosed area of charge versus voltage in fig.7(b) representing electrical energy output per cycle, increases accordingly.

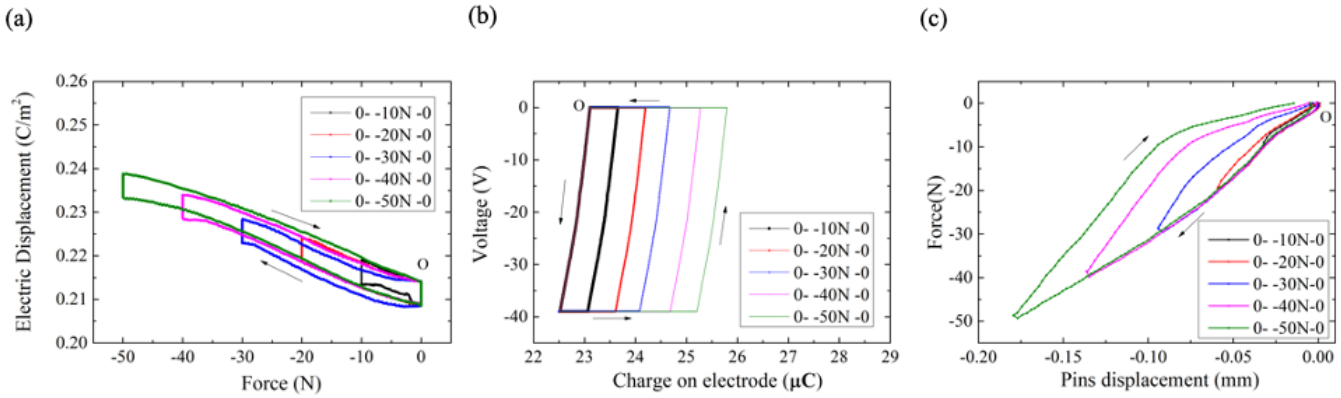

Figure 7. An example of energy harvesting cycle using compressive load stress with harvesting field -0.3E_0 for 30% pre-poled samples. (a) Electric displacement versus force. (b) Voltage versus charge on the electrode. (c) Force versus pins displacement.

The selection of force and electric field amplitude for maximum energy output in compression is next considered. The energy output per cycle and corresponding electric displacement change are shown versus force and electric field amplitude in fig. 8. In fig. 8(a), it is found that the energy output for the 100% pre-poled specimen increases monotonically with the rise of applied field strength, and the energy output per cycle reaches a maximum of 57 μJ in the range tested. As expected, high values of the harvesting electric field reduce the electric displacement change, see fig. 8(b), despite the energy output continuing to increase with electric field. In the fully polarized state very limited switching is possible; the observed electric displacement changes combine polarization switching and the piezoelectric effect. Greater electric displacement change and energy output can be observed in fig 8(c-h) with a maximum energy output per cycle of 115 μJ in the 30% pre-poled samples. As the degree of pre-poling is reduced,

the maximum energy output per cycle rises due to the increased freedom for polarization switching. A significant advantage of the compressive working mode is that the risk of cracking in the electroceramic during the energy harvesting cycle is greatly reduced: no cracking was observed in the range of parameters tested.

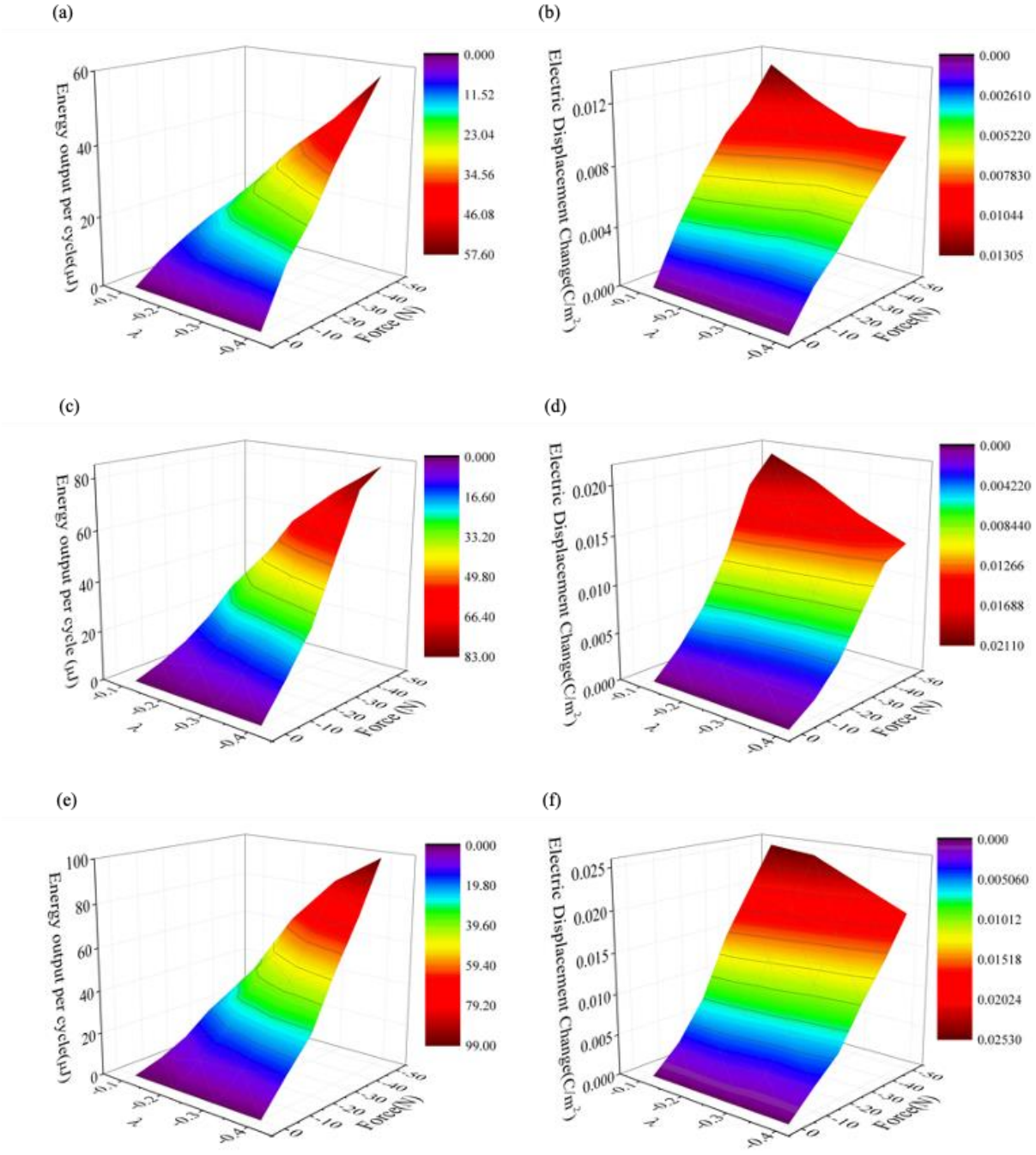

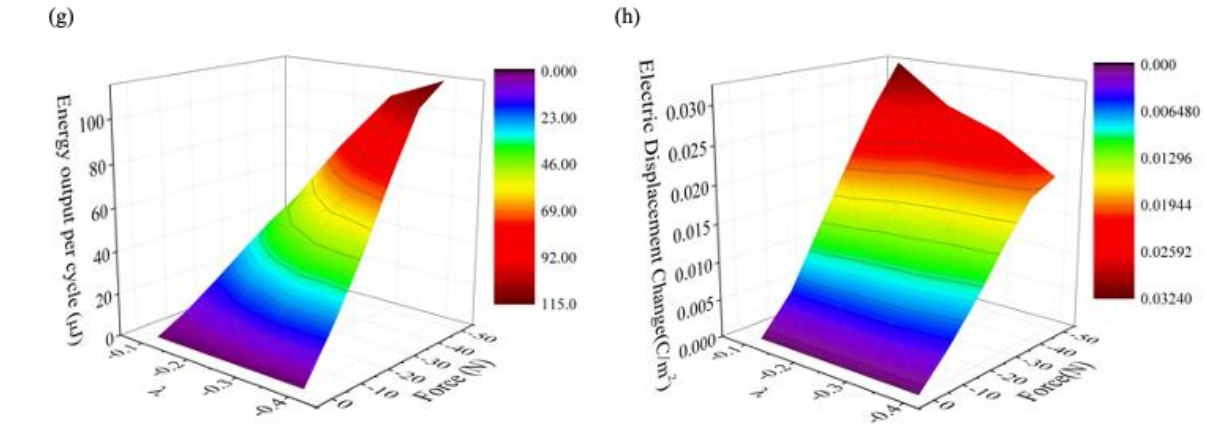

Figure 8. Energy output and electric displacement performance of the energy harvesters in compressive loading with various operating conditions: (a,c,e,g) Energy output per cycle versus peak force and harvesting electric field magnitude, (b,d,f,h) Corresponding magnitude of electric displacement change in each cycle. Pre-poling states as follows: (a,b) 100%, (c,d) 75% (e,f) 50% (g,h) 30%.

The energy output per cycle is an important performance metric for energy harvesting. However, when comparing different systems, volume scaling should be factored in. The ferroelectric/ferroelastic energy harvesters presented here achieved energy densities of 11 mJ/cm^3 and 3.2 mJ/cm^3 in tension and compression respectively. The system was operated in quasi-static conditions (<0.02 Hz); however, stable operation at frequencies up to 20Hz has been tested and appears viable. Other high-power piezoelectric [61-65] and triboelectric [53, 66-70] energy harvesters exhibit a wide range of cycle energy densities, from 0.005mJ/cm^3 up to about 10 mJ/cm^3. Thus the proposed system operates towards the top end of this range.

Another key factor for evaluating the working cycles is the energy conversion efficiency, which may vary from a few percent to more than 90%. To estimate the overall conversion efficiency, the input mechanical energy was computed from the enclosed area of the force versus loading pin displacement loops. Since the input energy calculated in this way includes frictional losses at the loading pins, as well as material and electrical losses in the energy harvester itself, the estimate gives an approximate measure, but can illustrate the typical efficiencies achieved. The resulting efficiencies are given for a range of operating parameters in Table 1. Since the same operating parameters were used with several different states of pre-poling, the table shows the range of efficiencies achieved in each operating state. In general it can be seen that an increase of amplitude of mechanical loading results in increased ferroelectric/ferroelastic switching, and thereby induces a drop in efficiency. In the few cases with 90% or more efficiency, the piezoelectric effect is dominant; these correspond to cases wherein the small amplitude of mechanical loading does not depolarise the electroceramic, when inhibited by the applied electric field. Furthermore, the mechanical work input needed for the compression mode is greater than that for the tension mode. Thus the efficiencies acquired in the compression working mode are typically lower than those of the tension mode. Further investigation of the conversion efficiency is a topic for future research.

Loading type	Load amplitude	Electric field	Measured
Tensile	10N	0.2	18-52%
Tensile	50N	0.2	10-25%
Tensile	10N	0.8	70-98%
Tensile	50N	0.8	30-67%
Compressive	10N	0.1	5-10%
Compressive	50N	0.1	2-3%
Compressive	10N	0.4	21-37%
Compressive	50N	0.4	4-6%

Table 1. Approximate efficiency of energy harvesting cycles at various amplitudes of mechanical and electrical loading.

5. Conclusion

The behaviour of ferroelectric wafers in partially poled states with residual stress was tested with a view to developing ferroelectric/ferroelastic energy harvesting cycles. The testing was quasi-static, and electric field was applied to simulate the impedance provided by an external electrical load. The experiments verify that the biased states of residual stress produced by the partial pre-poling process enable ferroelectric/ferroelastic switching to occur during the working cycle, and can guide the repolarization process under mechanical loading without the use of an external bias electric field to complete the energy harvesting cycle. The resulting devices have a simple structure and show much greater energy output per unit volume of active material than typical piezoelectrics. By varying the polarization state of the ferroelectric wafer, and the electrical and mechanical load amplitudes, a range of behaviour was explored. In general, reducing the extent of off-substrate pre-poling increased the energy output. However, this is also expected to increase the residual stresses and led to cracking in some cases. A 30% pre-poled sample gave a good balance of high energy output whilst avoiding degradation by cracking. While tensile loading gave the greatest energy output per cycle, compressive load cycles also yielded high energy density, with the advantage of greater robustness. The results demonstrate the basic working principle of a novel and practical ferroelectric/ferroelastic working cycle for mechanical to electrical energy conversion.

Acknowledgements

Wenbin Kang gratefully acknowledges support of the Jardine Foundation.

Competing Interests

The authors declare that they have no known competing financial interests or personal relationships that could have appeared to influence the work reported in this paper.

References

[1] F.K. Shaikh, S. Zeadally, Energy harvesting in wireless sensor networks: A comprehensive review, Renew. Sustain. Energy Rev. 55 (2016) 1041-1054.

[2] A. Nozariasbmarz, H. Collins, K. Dsouza, M.H. Polash, M. Hosseini, M. Hyland, J. Liu, A. Malhotra, F.M. Ortiz, F. Mohaddes, Review of wearable thermoelectric energy harvesting: From body temperature to electronic systems, Appl. Energy 258 (2020) 114069.

[3] M. Safaei, H.A. Sodano, S.R. Anton, A review of energy harvesting using piezoelectric materials: state-of-the-art a decade later (2008–2018), Smart Mater. Struct. 28(11) (2019) 113001.

[4] G. Zhang, M. Li, H. Li, Q. Wang, S. Jiang, Harvesting energy from human activity: ferroelectric energy harvesters for portable, implantable, and biomedical electronics, Energy Technol. 6(5) (2018) 791-812.

[5] H. Liu, J. Zhong, C. Lee, S.W. Lee, L. Lin, A comprehensive review on piezoelectric energy harvesting technology: Materials, mechanisms, and applications, Appl. Phys. Rev. 5(4) (2018) 041306.

[6] T.Y. Kim, S.K. Kim, S.W. Kim, Application of ferroelectric materials for improving output power of energy harvesters, Nano Converg. 5(1) (2018) 1-16.

[7] T. Yildirim, M.H. Ghayesh, W. Li, G. Alici, A review on performance enhancement techniques for ambient vibration energy harvesters, Renew. Sustain. Energy Rev. 71 (2017) 435-449.

[8] C. Wei, X. Jing, A comprehensive review on vibration energy harvesting: Modelling and realization, Renew. Sustain. Energy Rev. 74 (2017) 1-18.

[9] H. Liu, J. Zhong, C. Lee, S.-W. Lee, L. Lin, A comprehensive review on piezoelectric energy harvesting technology: Materials, mechanisms, and applications, Appl. Phys. Rev. 5(4) (2018) 041306.

[10] R. Ahmed, F. Mir, S. Banerjee, A review on energy harvesting approaches for renewable energies from ambient vibrations and acoustic waves using piezoelectricity, Smart Mater. Struct. 26(8) (2017) 085031.

[11] C.R. Bowen, V.Y. Topolov, H.A. Kim, Modern piezoelectric energy-harvesting materials, Springer 2016.

[12] Z. Yang, J. Zu, Comparison of PZN-PT, PMN-PT single crystals and PZT ceramic for vibration energy harvesting, Energy Convers. Manag. 122 (2016) 321-329.

[13] M. Rezaeisaray, M. El Gowini, D. Sameoto, D. Raboud, W. Moussa, Low frequency piezoelectric energy harvesting at multi vibration mode shapes, Sens. Actuator A Phys. 228 (2015) 104-111.

[14] B. Lee, S. Lin, W. Wu, X. Wang, P. Chang, C. Lee, Piezoelectric MEMS generators fabricated with an aerosol deposition PZT thin film, J. Micromech. Microeng. 19(6) (2009) 065014.

[15] S. Roundy, E.S. Leland, J. Baker, E. Carleton, E. Reilly, E. Lai, B. Otis, J.M. Rabaey, P.K. Wright, V. Sundararajan, Improving power output for vibration-based energy scavengers, IEEE Pervasive Comput. 4(1) (2005) 28-36.

[16] S.B. Kim, H. Park, S.H. Kim, H.C. Wikle, J.H. Park, D.J. Kim, Comparison of MEMS PZT cantilevers based on d_{31} and d_{33} modes for vibration energy harvesting, J. Microelectromech. Syst. 22(1) (2012) 26-33.

[17] N. Sharpes, A. Abdelkefi, S. Priya, Two-dimensional concentrated-stress low-frequency piezoelectric vibration energy harvesters, Appl. Phys. Lett. 107(9) (2015) 093901.

[18] M.A. Karami, D.J. Inman, Analytical modeling and experimental verification of the vibrations of the zigzag microstructure for energy harvesting, J. Vib. Acoust. 133(1) (2011).

[19] S. Kim, W.W. Clark, Q.M. Wang, Piezoelectric energy harvesting with a clamped circular plate: analysis, J. Intell. Mater. Syst. Struct. 16(10) (2005) 847-854.

[20] S.K. Ghosh, D. Mandal, Efficient natural piezoelectric nanogenerator: electricity generation from fish swim bladder, Nano Energy 28 (2016) 356-365.

[21] W. Wu, L. Wang, Y. Li, F. Zhang, L. Lin, S. Niu, D. Chenet, X. Zhang, Y. Hao, T.F. Heinz, Piezoelectricity of single-atomic-layer MoS 2 for energy conversion and piezotronics, Nature 514(7523) (2014) 470-474.

[22] B.Y. Lee, J. Zhang, C. Zueger, W.-J. Chung, S.Y. Yoo, E. Wang, J. Meyer, R. Ramesh, S.-W. Lee, Virus-based piezoelectric energy generation, Nat. Nanotechnol. 7(6) (2012) 351-356.

[23] G. Zhu, R. Yang, S. Wang, Z.L. Wang, Flexible high-output nanogenerator based on lateral ZnO nanowire array, Nano Lett. 10(8) (2010) 3151-3155.

[24] Y. Qi, M.C. McAlpine, Nanotechnology-enabled flexible and biocompatible energy harvesting, Energy Environ. Sci. 3(9) (2010) 1275-1285.
[25] D. Vasilescu, R. Cornillon, G. Mallet, Piezoelectric resonances in amino-acids, Nature 225(5233) (1970) 635-635.
[26] L. Staaf, A. Smith, E. Köhler, P. Lundgren, P. Folkow, P. Enoksson, Achieving increased bandwidth for 4 degree of freedom self-tuning energy harvester, J. Sound Vib. 420 (2018) 165-173.
[27] S. Dhote, Z. Yang, J. Zu, Modeling and experimental parametric study of a tri-leg compliant orthoplanar spring based multi-mode piezoelectric energy harvester, Mech. Syst. Signal Process. 98 (2018) 268-280.
[28] J. Iannacci, G. Sordo, E. Serra, U. Schmid, The MEMS four-leaf clover wideband vibration energy harvesting device: design concept and experimental verification, Microsyst. Technol. 22(7) (2016) 1865-1881.
[29] H. Wang, F. Hu, K. Wang, Y. Liu, W. Zhao, Three-dimensional piezoelectric energy harvester with spring and magnetic coupling, Appl. Phys. Lett. 110(16) (2017) 163905.
[30] N. Zhao, J. Yang, Q. Yu, J. Zhao, J. Liu, Y. Wen, P. Li, Three-dimensional piezoelectric vibration energy harvester using spiral-shaped beam with triple operating frequencies, Rev. Sci. Instrum. 87(1) (2016) 015003.
[31] R. Chen, L. Ren, H. Xia, X. Yuan, X. Liu, Energy harvesting performance of a dandelion-like multi-directional piezoelectric vibration energy harvester, Sens. Actuator A Phys. 230 (2015) 1-8.
[32] L. Tang, Y. Yang, A nonlinear piezoelectric energy harvester with magnetic oscillator, Appl. Phys. Lett. 101(9) (2012) 094102.
[33] G. Sebald, H. Kuwano, D. Guyomar, B. Ducharne, Experimental Duffing oscillator for broadband piezoelectric energy harvesting, Smart Mater. Struct. 20(10) (2011) 102001.
[34] K.Q. Fan, F.B. Chao, J.G. Zhang, W.D. Wang, X.H. Che, Design and experimental verification of a bi-directional nonlinear piezoelectric energy harvester, Energy Convers. Manag. 86 (2014) 561-567.
[35] R. Harne, M. Thota, K. Wang, Concise and high-fidelity predictive criteria for maximizing performance and robustness of bistable energy harvesters, Appl. Phys. Lett. 102(5) (2013) 053903.
[36] A. Erturk, J. Hoffmann, D.J. Inman, A piezomagnetoelastic structure for broadband vibration energy harvesting, Appl. Phys. Lett. 94(25) (2009) 254102.
[37] B. Andò, S. Baglio, A.R. Bulsara, V. Marletta, A. Pistorio, Investigation of a nonlinear energy harvester, IEEE Trans. Instrum. Meas. 66(5) (2017) 1067-1075.
[38] Y. Kuang, M. Zhu, Design study of a mechanically plucked piezoelectric energy harvester using validated finite element modelling, Sens. Actuator A Phys. 263 (2017) 510-520.
[39] X. Zhang, S. Gao, D. Li, L. Jin, Q. Wu, F. Liu, Frequency up-converted piezoelectric energy harvester for ultralow-frequency and ultrawide-frequency-range operation, Appl. Phys. Lett. 112(16) (2018) 163902.
[40] H. Fu, E.M. Yeatman, A methodology for low-speed broadband rotational energy harvesting using piezoelectric transduction and frequency up-conversion, Energy 125 (2017) 152-161.
[41] Y. Sang, X. Huang, H. Liu, P. Jin, A vibration-based hybrid energy harvester for wireless sensor systems, IEEE Trans. Magn. 48(11) (2012) 4495-4498.
[42] V.R. Challa, M. Prasad, F.T. Fisher, A coupled piezoelectric–electromagnetic energy harvesting technique for achieving increased power output through damping matching, Smart Mater. Struct. 18(9) (2009) 095029.
[43] M. Rezaei, R. Talebitooti, S. Rahmanian, Efficient energy harvesting from nonlinear vibrations of PZT beam under simultaneous resonances, Energy 182 (2019) 369-380.
[44] P. Shirazi, G. Ico, C.S. Anderson, M.C. Ma, B.S. Kim, J. Nam, N.V. Myung, Size-Dependent Piezoelectric Properties of Electrospun BaTiO3 for Enhanced Energy Harvesting, Adv. Sustain. Syst. 1(11) (2017) 1700091.
[45] X. Chen, X. Han, Q.D. Shen, PVDF-based ferroelectric polymers in modern flexible electronics, Adv. Electron. Mater. 3(5) (2017) 1600460.
[46] A. Alomari, A. Batra, M. Aggarwal, C. Bowen, A multisource energy harvesting utilizing highly efficient ferroelectric PMN-PT single crystal, J. Mater. Sci.: Mater. Electron. 27(10) (2016) 10020-10030.

[47] Y. Zhang, P.T.T. Phuong, E. Roake, H. Khanbareh, Y. Wang, S. Dunn, C. Bowen, Thermal energy harvesting using pyroelectric-electrochemical coupling in ferroelectric materials, Joule 4(2) (2020) 301-309.
[48] H. Tang, X.-G. Tang, M.-D. Li, Q.-X. Liu, Y.-P. Jiang, Pyroelectric energy harvesting capabilities and electrocaloric effect in lead-free SrxBa1-xNb2O6 ferroelectric ceramics, J. Alloys Compd. 791 (2019) 1038-1045.
[49] H. Röhm, T. Leonhard, A.D. Schulz, S. Wagner, M.J. Hoffmann, A. Colsmann, Ferroelectric properties of perovskite thin films and their implications for solar energy conversion, Adv. Mater. 31(26) (2019) 1806661.
[50] Y. Bai, H. Jantunen, J. Juuti, Ferroelectric Oxides for Solar Energy Conversion, Multi-Source Energy Harvesting/Sensing, and Opto-Ferroelectric Applications, ChemSusChem 12(12) (2019) 2540.
[51] S. Pandya, J. Wilbur, J. Kim, R. Gao, A. Dasgupta, C. Dames, L.W. Martin, Pyroelectric energy conversion with large energy and power density in relaxor ferroelectric thin films, Nat. Mater. 17(5) (2018) 432-438.
[52] X. Wang, S. Niu, F. Yi, Y. Yin, C. Hao, K. Dai, Y. Zhang, Z. You, Z.L. Wang, Harvesting ambient vibration energy over a wide frequency range for self-powered electronics, ACS Nano 11(2) (2017) 1728-1735.
[53] J. Wang, C. Wu, Y. Dai, Z. Zhao, A. Wang, T. Zhang, Z.L. Wang, Achieving ultrahigh triboelectric charge density for efficient energy harvesting, Nat. Commun. 8(1) (2017) 1-8.
[54] L. Behlen, A. Warkentin, A. Ricoeur, Exploiting ferroelectric and ferroelastic effects in piezoelectric energy harvesting: theoretical studies and parameter optimization, Smart Mater. Struct. 30(3) (2021) 035031.
[55] W. Kang, J.E. Huber, Prospects for energy harvesting using ferroelectric/ferroelastic switching, Smart Mater. Struct. 28(2) (2019) 024002.
[56] D. Wang, R. Melnik, L. Wang, Material influence in newly proposed ferroelectric energy harvesters, J. Intell. Mater. Syst. Struct. 29(16) (2018) 3305-3316.
[57] D. Wang, L. Wang, R. Melnik, Vibration energy harvesting based on stress-induced polarization switching: a phase field approach, Smart Mater. Struct. 26(6) (2017) 065022.
[58] A.R. Balakrishna, J.E. Huber, Nanoscale domain patterns and a concept for an energy harvester, Smart Mater. Struct. 25(10) (2016) 104001.
[59] S. Hwang, C. Lynch, R. McMeeking, Ferroelectric/ferroelastic interactions and a polarization switching model, Acta Metall. Mater. 43(5) (1995) 2073-2084.
[60] C.S. Lynch, The effect of uniaxial stress on the electro-mechanical response of 8/65/35 PLZT, Acta Mater. 44(10) (1996) 4137-4148.
[61] X. Gao, J. Wu, Y. Yu, Z. Chu, H. Shi, S. Dong, Giant piezoelectric coefficients in relaxor piezoelectric ceramic PNN-PZT for vibration energy harvesting, Adv. Funct. Mater. 28(30) (2018) 1706895.
[62] Y. Yue, Y. Hou, M. Zheng, X. Yan, J. Fu, M. Zhu, High power density in a piezoelectric energy harvesting ceramic by optimizing the sintering temperature of nanocrystalline powders, J. Eur. Ceram. Soc. 37(15) (2017) 4625-4630.
[63] Q. Zheng, H. Zhang, H. Mi, Z. Cai, Z. Ma, S. Gong, High-performance flexible piezoelectric nanogenerators consisting of porous cellulose nanofibril (CNF)/poly (dimethylsiloxane)(PDMS) aerogel films, Nano Energy 26 (2016) 504-512.
[64] S. Siddiqui, D.I. Kim, M.T. Nguyen, S. Muhammad, W.S. Yoon, N.E. Lee, High-performance flexible lead-free nanocomposite piezoelectric nanogenerator for biomechanical energy harvesting and storage, Nano Energy 15 (2015) 177-185.
[65] W. Jin, Z. Wang, H. Huang, X. Hu, Y. He, M. Li, L. Li, Y. Gao, Y. Hu, H. Gu, High-performance piezoelectric energy harvesting of vertically aligned $Pb(Zr,Ti)O_3$ nanorod arrays, RSC Adv. 8(14) (2018) 7422-7427.
[66] W. He, W. Liu, J. Chen, Z. Wang, Y. Liu, X. Pu, H. Yang, Q. Tang, H. Yang, H. Guo, Boosting output performance of sliding mode triboelectric nanogenerator by charge space-accumulation effect, Nat. Commun. 11(1) (2020) 1-8.
[67] D. Tantraviwat, P. Buarin, S. Suntalelat, W. Sripumkhai, P. Pattamang, G. Rujijanagul, B. Inceesungvorn, Highly dispersed porous polydimethylsiloxane for boosting power-generating performance of triboelectric nanogenerators, Nano Energy 67 (2020) 104214.

571 [68] W. Liu, Z. Wang, G. Wang, G. Liu, J. Chen, X. Pu, Y. Xi, X. Wang, H. Guo, C. Hu, Integrated
572 charge excitation triboelectric nanogenerator, Nat. Commun. 10(1) (2019) 1-9.
573 [69] Y. Bai, L. Xu, S. Lin, J. Luo, H. Qin, K. Han, Z.L. Wang, Charge pumping strategy for rotation
574 and sliding type triboelectric nanogenerators, Adv. Energy Mater. 10(21) (2020) 2000605.
575 [70] H. Wang, L. Xu, Y. Bai, Z.L. Wang, Pumping up the charge density of a triboelectric nanogenerator
576 by charge-shuttling, Nat. Commun. 11(1) (2020) 1-9.
577